Journal of Solid State Chemistry 181 (2008) 2448–2455

Contents lists available at ScienceDirect

Journal of Solid State Chemistry

journal homepage: www.elsevier.com/locate/jssc

Yb_3CoSn_6 and $Yb_4Mn_2Sn_5$: New polar intermetallics with 3D open-framework structures

Xiao-Wu Lei [a,b], Guo-Hua Zhong [a,b], Min-Jie Li [a,b], Jiang-Gao Mao [a,*]

[a] State Key Laboratory of Structural Chemistry, Fujian Institute of Research on the Structure of Matter, Chinese Academy of Sciences, Fuzhou, Fujian 350002, PR China
[b] The Graduate School of the Chinese Academy of Sciences, Beijing 100039, PR China

ARTICLE INFO

Article history:
Received 19 February 2008
Received in revised form
21 May 2008
Accepted 27 May 2008
Available online 10 July 2008

Keywords:
Polar intermetallics
Solid-state synthesis
Crystal structure
Stannide
Band structure calculation

ABSTRACT

Two new ternary ytterbium transition metal stannides, namely, Yb_3CoSn_6 and $Yb_4Mn_2Sn_5$, have been obtained by solid-state reactions of the corresponding pure elements in welded tantalum tubes at high temperature. Their crystal structures have been established by single-crystal X-ray diffraction studies. Yb_3CoSn_6 crystallizes in the orthorhombic space group *Cmcm* (no. 63) with cell parameters of $a = 4.662(2)$, $b = 15.964(6)$, $c = 13.140(5)$ Å, $V = 978.0(6)$ Å^3, and $Z = 4$. Its structure features a three-dimensional (3D) open-framework composed of unusual $[CoSn_3]$ layers interconnected by zigzag Sn chains, forming large tunnels along the *c*-axis which are occupied by the ytterbium cations. $Yb_4Mn_2Sn_5$ is monoclinic space group *C*2/*m* (no. 12) with cell parameters of $a = 16.937(2)$, $b = 4.5949(3)$, $c = 7.6489(7)$ Å, $\beta = 106.176(4)^\circ$, $V = 571.70(8)$ Å^3, and $Z = 2$. It belongs to the Mg_5Si_6 structure type and its anionic substructure is composed of parallel $[Mn_2Sn_2]$ ladders interconnected by unusual zigzag $[Sn_3]$ chains, forming large tunnels along the *c*-axis, which are filled by the ytterbium cations. Band structure calculations based on density function theory methods were also made for both compounds.

1. Introduction

Polar intermetallics formed between alkali metal (or alkaline earth metal or rare-earth metal) and tin element are of considerable research interest in recent years, mainly due to their richness in structural chemistry and tunable electronic properties [1–10]. For example, $SrSn_3$, $BaSn_3$, $SrSn_4$, and $BaSn_5$ display superconductivity below 5.4, 2.4, 4.8, and 4.4 K, respectively [11–14]. Furthermore, various tin-rich phases containing two types of cations with different sizes exhibit various unusual anionic clusters or clathrate cages based on tin pentagons and possess interesting thermoelectric properties [15–22].

Transition metals have abundant *d* orbital electrons, and their Pauling's electronegativities are close to that of tin, hence the introduction of transition metals in these *A*-Sn (*A* represents alkali, alkaline earth, or rare-earth metal) binary systems can dramatically change their structures, electronic and magnetic properties as well as improve their thermal stabilities [23,24]. Rare-earth copper stannides have been widely investigated due to their interesting physical properties, such as $Yb_3Cu_6Sn_5$, $Yb_3Cu_8Sn_4$, $Yb_4Cu_2Sn_5$, and $Gd_3Cu_4Sn_4$ [25–27]. As for the *A*-Ni–Sn ternary system, a variety of reported phases include $BaNiSn_3$, $MgNi_2Sn$, $Ca_7Ni_4Sn_{13}$, $Ce_3Ni_2Sn_7$, $La_{4.87}Ni_{12}Sn_{24}$, and Sm_2NiSn_4 [28–33]. Several *RE*-Co(Mn)–Sn ternary phases have also been prepared including Ce_2CoSn_2, $RE_3Co_8Sn_4$ (RE = Y, Pr, Nd, Sm, Gd–Lu), $RE_3Co_6Sn_5$ (RE = Y, Nd, Sm, Gd, Tb, Ho–Tm) and $YbMn_6Sn_6$ [34–38]. In many of ternary phases, it is interesting to note that Sn atoms tend to form Sn_4 squares capped by transition metals, resulting in various 2D layers which are interconnected by zigzag Sn chains into various 3D open frameworks. For example, compounds with the $DyCoSn_2$ structure type display 2D [TMSn] layers composed of tin square sheets capped by transition metal atoms alternatively above and below which are further interconnected by 1D zigzag Sn chains into a 3D open framework [39–41]. The structure of Sm_2NiSn_4 features a two-dimensional (2D) corrugated $[NiSn_4]$ anionic layer composed of 2D $[NiSn_2]$ layers attached by 1D zigzag Sn chains as side arms, half of the Sn square sheets are capped by Ni atoms above and below. Packing of such layers results in pseudo-tunnels occupied by Sm atoms [33].

However, much more systematic research works are needed to understand the structures, chemical bonding and physical properties of these *A*-TM–Sn ternary phases. Our exploration of new phases in Yb–Co(Mn)–Sn ternary systems led to two new ytterbium transition metal stannides, namely, Yb_3CoSn_6 and $Yb_4Mn_2Sn_5$. Herein, we report their syntheses, crystal structures and band structures.

* Corresponding author. Fax: +86 591 83714946.
E-mail address: mjg@fjirsm.ac.cn (J.-G. Mao).

0022-4596/$ - see front matter © 2008 Elsevier Inc. All rights reserved.
doi:10.1016/j.jssc.2008.05.036

2. Experimental section

2.1. Materials and instrumentation

All manipulations were performed inside an argon-filled glove box with moisture level below 1 ppm. The metals used were ytterbium blocks (Acros, 99.99%), cobalt and manganese powder (Tianjin Fuchen chemical reagent company, 99.99%), and tin granules (Acros, 99.999%). Elemental analyses for Yb, Co, Mn, and Sn were performed on an energy dispersive X-ray spectroscope (EDS, Oxford INCA) attached to the FESEM. Data were acquired with an accelerating voltage of 20 kV and SEM of 40°. X-ray powder diffraction patterns were collected on an X'Pert-Pro diffractometer using Cu$K\alpha$ radiation ($\lambda = 1.5406$ Å) in the 2θ range of 5–85°. The generator voltage was 45 kV and the tube current was 40 mA.

2.2. Preparation of Yb_3CoSn_6

Single crystals of Yb_3CoSn_6 were initially obtained by the solid-state reaction of the corresponding pure elements in a molar ratio of 3:1:6 (Yb:Co:Sn). The mixture was loaded into a tantalum tube, which was subsequently arc-welded under an argon atmosphere and sealed into an evacuated quartz tube ($\sim 10^{-4}$ Torr). The sample was heated at 300 °C for 1 day and then 1000 °C for 7 days, and then it was allowed to cool slowly (6 °C/h) to room temperature. Silver sheet-like crystals of Yb_3CoSn_6 were selected and used for structure determination. Microprobe analyses on several single crystals indicated the presence of Yb, Co, and Sn in a molar ratio of 3.2(3): 1.0(3): 6.4(6), which was in good agreement with the results from single crystal X-ray diffraction studies. The crystals of Yb_3CoSn_6 were very brittle and slightly sensitive to air and hydrosphere. After the structural analyses, attempts were made to prepare a mono phase of Yb_3CoSn_6 by the reactions of the stoichiometric mixture of the pure metals in Ta tubes under different temperatures. The highest yields of about 90% were obtained by heating samples at 1000 °C for 2 days, quenched in water and then annealed at 650 °C for 2 weeks. The impurity phases included YbSn ($P4/mmm$) and $YbSn_3$ ($Pm\bar{3}m$).

2.3. Preparation of $Yb_4Mn_2Sn_5$

Single crystals of $Yb_4Mn_2Sn_5$ were initially obtained in our attempt to prepare the Mn analog of Yb_3CoSn_6. The sample was first heated at 300 °C for 1 day and then at 980 °C for 7 days, then it was allowed to cool slowly (6 °C/h) to room temperature. The silver gray, prism-shaped crystals of $Yb_4Mn_2Sn_5$ were selected and used for structural determination. Microprobe elemental analyses on several single crystals gave a chemical composition of $Yb_{4.1(4)}Mn_{2.0(3)}Sn_{5.4(5)}$, which was close to that from single crystal structural determination. After the structural analyses, a lot of efforts were made to synthesize the mono-phase product of $Yb_4Mn_2Sn_5$ by reacting a stoichiometric mixture of the pure metals in welded Ta tubes under various temperatures such as 1000, 950, 900, 850, and 700 °C. However, the measured X-ray powder patterns of the resultant products revealed the presence of several impurity phases, such as YbSn ($P4/mmm$), $YbSn_3$ ($Pm\bar{3}m$) as well as other unidentified compounds. The highest purity of about 85% was obtained by heating sample at 1000 °C for 2 days, quenching in cold water and then annealed at 570 °C for 2 weeks. Attempts to prepare $Ca_4Mn_2Sn_5$ and $Yb_4Co_2Sn_5$ analogies were tried but unsuccessful.

2.4. Crystal structure determination

Single crystals of Yb_3CoSn_6 and $Yb_4Mn_2Sn_5$ were selected from the bulk reaction products and sealed into the thin-walled glass capillaries. Data collection for both compounds was performed on a Rigaku Mercury CCD (CCD stands for Charge-Coupled Device, Mo$K\alpha$ radiation, graphite monochromator) at 293(2) K. Both data sets were corrected for Lorentz factor, polarization, air absorption and absorption due to variations in the path length through the detector faceplate. Absorption corrections based on Multi-scan method were also applied [42]. A total of 645 and 728 independent reflections for Yb_3CoSn_6 and $Yb_4Mn_2Sn_5$, respectively, were measured, of which 529 and 589 reflections with $I > 2\sigma(I)$ were considered observed.

Both structures were solved by using direct methods (SHELXTL) and refined by least-squares methods with atomic coordinates and anisotropic thermal parameters [43]. All atomic sites in both compounds were fully occupied according to the site occupancy refinements. Final difference Fourier maps showed featureless residual peaks of 3.82 and -3.65 e Å^{-3} (0.71 and 1.04 Å from Yb(1) and Yb(2), respectively) for Yb_3CoSn_6, and 3.58 and -3.51 e Å^{-3} (0.82 and 0.97 Å, respectively, away from Yb(1)) for $Yb_4Mn_2Sn_5$. Some of the data collection and refinement parameters are summarized in Table 1. Atomic coordinates and important bond lengths and angles are listed in Tables 2 and 3, respectively.

Crystallographic data in CIF format for Yb_3CoSn_6 and $Yb_4Mn_2Sn_5$ have been given as Supporting Materials. These data can also be obtained from the Fachinformationszentrum Karlsruhe, 76344 Eggenstein-Leopoldshafen, Germany (fax: +49 7247 808 666; e-mail: crysdata@fiz-karlsruhe.de) on quoting the depository numbers CSD 419133 and 419134.

2.5. Electronic structure calculations

Band structure calculations for Yb_3CoSn_6 and $Yb_4Mn_2Sn_5$ were performed using the highly accurate full-potential linearized-augmented plane wave plus local basis (FLAPW+lo) method within density functional theory (DFT), using the general gradient approximation (GGA) of Perdew–Burke–Ernzerhof (PBE) version to treat the exchange and correlation potential [44–46]. The calculations were implemented using the WIEN2k code [47].

The calculation sets were based on the primitive cell for Yb_3CoSn_6 ($Z = 2$) and $Yb_4Mn_2Sn_5$ ($Z = 1$). In order to obtain as

Table 1
Summary of cell parameters, data collection, and structure refinements for Yb_3CoSn_6 and $Yb_4Mn_2Sn_5$

Chemical formula	Yb_3CoSn_6	$Yb_4Mn_2Sn_5$
Fw	1290.19	1395.49
Space group	$Cmcm$ (no. 63)	$C2/m$ (no. 12)
a (Å)	4.662(2)	16.937(2)
b (Å)	15.964(6)	4.5949(3)
c (Å)	13.140(5)	7.6489(7)
β (deg)	90	106.176(4)
V (Å^3)	978.0(6)	571.70(8)
Z	4	2
D_{calcd} (g/cm^3)	8.762	8.107
Temp (K)	293(2)	293(2)
μ (Mo$K\alpha$) mm^{-1}	44.977	45.125
Crystal size (mm)	$0.1 \times 0.1 \times 0.02$	$0.2 \times 0.02 \times 0.02$
Color and habit	Black, sheet	Gray, prism
$h\,k\,l$ range	(−6, 5), (−15, 20), (−16, 17)	(−19, 21), ±5, ±9
Reflections collected	3754	2207
Unique reflections	645	728
Reflections ($I > 2\sigma(I)$)	529	589
GOF on F^2	1.033	0.861
$R1$, w$R2$ ($I > 2\sigma(I)$)[a]	0.0442/0.0945	0.0340/0.0779
$R1$, w$R2$ (all data)	0.0478/0.0955	0.0385/0.0789

[a] $R1 = \sum||F_o|-|F_c||/\sum|F_o|$, w$R2 = \{\sum w[(F_o)^2-(F_c)^2]^2/\sum w[(F_o)^2]^2\}^{1/2}$.

Table 2
Atomic coordinates and equivalent thermal parameters ($\times 10^3$ Å^2) for Yb_3CoSn_6 and $Yb_4Mn_2Sn_5$

Atom	Wyck	x	y	z	U(eq)[a]
Yb_3CoSn_6					
Yb(1)	4c	1/2	0.4022(1)	3/4	10(1)
Yb(2)	8f	1/2	0.5978(1)	0.5962(1)	11(1)
Co(1)	4c	1/2	0.2040(2)	3/4	9(1)
Sn(1)	8f	1/2	0.2545(1)	0.5699(1)	14(1)
Sn(2)	4c	0	0.2688(1)	3/4	11(1)
Sn(3)	8f	0	0.4277(1)	0.5771(1)	12(1)
Sn(4)	4c	0	0.5451(1)	3/4	9(1)
$Yb_4Mn_2Sn_5$					
Yb(1)	4i	0.1501(1)	0	0.4313(1)	12(1)
Yb(2)	4i	0.0771(1)	0	0.8570(1)	12(1)
Mn(1)	4i	0. 2767(2)	0	0. 8885(4)	10(1)
Sn(1)	4i	0.0666(1)	1/2	0. 1590(2)	10(1)
Sn(2)	2c	0	1/2	1/2	13(1)
Sn(3)	4i	0.3077(1)	0	0. 2665(2)	10(1)

[a] U(eq) is defined as one-third of the trace of the orthogonalized U_{ij} tensor.

Table 3
Selected bond lengths (Å) and angles (deg) for Yb_3CoSn_6 and $Yb_4Mn_2Sn_5$

Yb_3CoSn_6			
Yb(1)–Sn(2)	3.157(2) × 2	Yb(1)–Co(1)	3.164(3)
Yb(1)–Sn(4)	3.263(2) × 2	Yb(1)–Sn(3)	3.281(1) × 4
Yb(1)–Sn(1)	3.340(2) × 2	Yb(2)–Sn(4)	3.197(1) × 2
Yb(2)-Sn(1)	3.214(2)	Yb(2)–Sn(3)	3.284(1) × 2
Yb(2)–Sn(2)	3.397(2)	Yb(2)–Sn(1)	3.437(1) × 2
Yb(2)–Co(1)	3.520(2) × 2	Yb(2)–Sn(3)	3.587(1) × 2
Co(1)–Sn(1)	2.500(2) × 2	Co(1)–Sn(4)	2.536(4)
Co(1)–Sn(2)	2.550(2) × 2	Sn(1)–Sn(1)	2.972(2) × 2
Sn(3)–Sn(4)	2.945(2)	Sn(3)–Sn(3)	3.071(3)
Sn(1)–Co(1)–Sn(1)	142.4(2)	Sn(1)–Co(1)–Sn(4)	108.81(8) × 2
Sn(1)–Co(1)–Sn(2)	82.48(5) × 4	Sn(4)–Co(1)–Sn(2)	113.94(7) × 2
Sn(2)–Co(1)–Sn(2)	132.1(2)	Sn(1)–Sn(1)–Sn(1)	103.34(8)
Co(1)–Sn(2)–Co(1)	132.1(2)	Co(1)–Sn(4)–Sn(3)	129.52(4) × 2
Sn(3)–Sn(4)–Sn(3)	100.96(8)	Sn(4)–Sn(3)–Sn(3)	91.77(7)
$Yb_4Mn_2Sn_5$			
Yb(1)–Sn(1)	3.158(1) × 2	Yb(1)–Sn(3)	3.196(1) × 2
Yb(1)–Sn(3)	3.254(2)	Yb(1)–Mn(1)	3.557(3)
Yb(1)–Sn(2)	3.572(7) × 2	Yb(1)–Mn(1)	3.806(2) × 2
Yb(2)–Sn(1)	3.298(1) × 2	Yb(2)–Sn(3)	3.318(1) × 2
Yb(2)–Mn(1)	3.322(3)	Yb(2)–Sn(1)	3.324(1) × 2
Yb(2)–Sn(2)	3.529(7) × 2	Yb(2)–Mn(1)	3.537(2) × 2
Mn(1)–Sn(1)	2.777(3)	Mn(1)–Sn(3)	2.790(2) × 2
Mn(1)–Sn(3)	2.791(3)	Mn(1)–Mn(1)	3.142(4) × 2
Sn(1)–-Sn(1)	2.819(3)	Sn(1)–Sn(2)	3.117(1)
Sn(2)–Sn(3)	3.250(1) × 2		
Sn(1)–Mn(1)–Sn(3)	109.86(7) × 2	Sn(3)–Mn(1)–Sn(3)	110.9(1)
Sn(1)–Mn(1)–Sn(3)	103.0(1)	Sn(3)–Mn(1)–Sn(3)	111.47(7) × 2
Sn(1)–Sn(1)–Sn(2)	109.46(6)	Sn(1)–Sn(2)–Sn(1)	180.00(4)
Sn(1)–Sn(2)–Sn(3)	94.64(3) × 2	Sn(1)–Sn(2)–Sn(3)	85.36(3) × 2
Sn(3)–Sn(2)–Sn(3)	180.0	Mn(1)–Sn(3)–Mn(1)	110.9(1)
Mn(1)–Sn(3)–Mn(1)	68.53(7) × 2		

precise calculation results as possible, we have set $R_{MT}K_{MAX} = 7$, where K_{MAX} is the maximum modulus for the reciprocal lattice vector, and R_{MT} is the muffin-tin (MT) spherical radius present in the system. These values of 2.5, 2.49, 2.45, and 2.21 Å for Yb, Co, Mn, and Sn are used as the MT radii, respectively. Integrations in the irreducible Brillouin zone have been performed using the standard tetrahedron-method. The charge convergence of the self-consistent iterations is to 0.0001 with a cutoff energy of −8.0 Ry between the valence and the core states. The 4*f*, 5*d*, 6*s* orbitals for Yb, 3*d*, 4*s* orbitals for Co and Mn, and 5*s*, 5*p* orbitals for Sn atoms are regarded as valence states, respectively.

3. Results and discussion

3.1. Structural descriptions

Exploratory syntheses in the *RE*-Co(Mn)–Sn ternary systems led to two new polar intermetallic compounds, Yb_3CoSn_6 and $Yb_4Mn_2Sn_5$. Both compounds feature three-dimensional (3D) anionic open-frameworks.

Yb_3CoSn_6 features a 3D anionic open framework built by $[CoSn_3]$ layers interconnected by 1D zigzag Sn chains, forming large tunnels along the *c*-axis, which are occupied by the Yb cations (Fig. 1)

The $[CoSn_3]$ layer is formed by square sheet of Sn(1) and Sn(2) atoms with one-third of the Sn_4 squares being capped by Co(1) atoms alternatively on both sides. Co(1) is 0.92 Å off the plane formed by two Sn(1) and two Sn(2) atoms (Fig. 2a). It is noted that the tin squares are severely distorted and exhibit two types of Sn–Sn distances: Sn(1)–Sn(1) bond of 2.972(2) Å and Sn(1)–Sn(2) bond of 3.330(2) Å. The former is slightly longer than the Sn–Sn single bond distance of 2.810 Å observed in element α-tin [48] whereas the latter is close to that reported for the tin square sheets in $BaMg_2Sn_2$, which could be considered as a weak bonding interaction [49]. The Co–Sn distances fall in the range of 2.500(2)–2.550(2) Å, which are comparable with those reported in $RE_4Co_2Sn_5$ (*RE* = La, Ce), $Ca_7Co_8Sn_{25}$, $RE_3Co_4Sn_{13}$ (*RE* = La, Ce, Yb), $Mg_2Co_3Sn_{10+x}$ ($0 \leqslant x \leqslant 0.15$) and $YbCo_6Sn_6$, but significantly

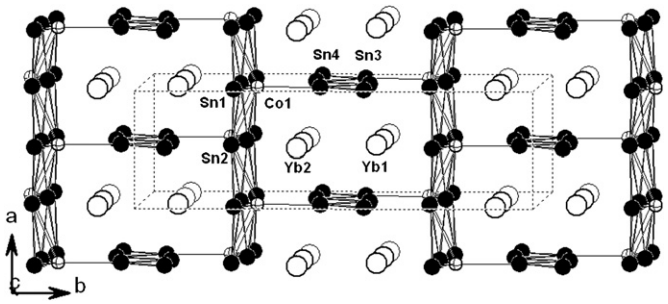

Fig. 1. View of the structure of Yb_3CoSn_6 down the *c*-axis (b). Yb, Co, and Sn atoms are drawn as open, crossed, and black circles, respectively. The unit cell edges are drawn as dashed lines.

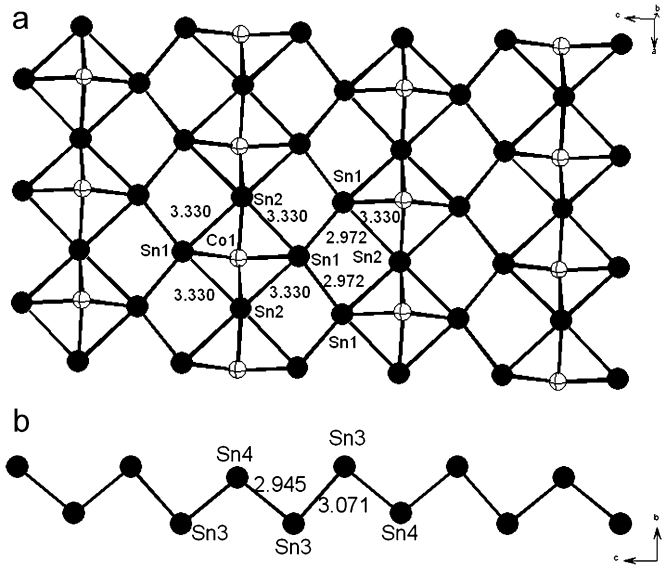

Fig. 2. A $[CoSn_3]$ layer parallel to the ac plane (a) and a 1D zigzag chain of tin along the *c*-axis (b) in Yb_3CoSn_6.

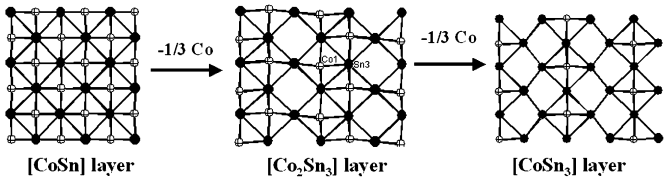

Fig. 3. Comparison of the [CoSn] layer in $DyCoSn_2$ with the $[Co_2Sn_3]$ layer in $Ce_4Co_2Sn_5$, and the $[CoSn_3]$ layer in Yb_3CoSn_6.

shorter than those reported in the Co–Sn binary phases (2.618–2.737 Å) [50–58]. It is interesting to compare the $[CoSn_3]$ layer in Yb_3CoSn_6 with the [CoSn] layer in $DyCoSn_2$ and the $[Co_2Sn_3]$ layer in $Ce_4Co_2Sn_5$ (Fig. 3) [39,50]. All of them feature Sn square sheets capped by Co atoms alternatively above and below. The Sn squares are completely capped by Co atoms for the [CoSn] layer in $DyCoSn_2$, whereas only two-thirds and one-third of the Sn squares are capped by Co atoms for the $[Co_2Sn_3]$ layer in $Ce_4Co_2Sn_5$ and the $[CoSn_3]$ layer in Yb_3CoSn_6, respectively.

The zigzag Sn chain formed by Sn(3) and Sn(4) atoms is similar to those in Sm_2NiSn_4 and EuSn (Fig. 2b) [33,59]. Within the chain, the Sn(3)–Sn(3) bond of 3.071(3) Å is little longer than the Sn(3)–Sn(4) bond of 2.945(2) Å, and the Sn(3)–Sn(4)–Sn(3) angle of 100.96(8)° is significantly larger than that of Sn(4)–Sn(3)–Sn(3) (91.77(7)°).

The $[CoSn_3]$ layers and zigzag $[Sn_3]$ chains are further interconnected via Co(1)–Sn(4) bonds (2.536(4) Å) into a novel 3D open framework with long large tunnels along the *c*-axis. The ytterbium cations are located at the above tunnels (Fig. 1). Yb(1) is 11-coordinated by one Co and 10 Sn atoms whereas Yb(2) is surrounded by two Co and 10 Sn atoms. The Yb–Co and Yb–Sn distances are in the ranges of 3.164(3)–3.520(2) Å and 3.157(2)–3.587(1) Å, respectively, which are comparable with those in $Yb_3Co_4Sn_{13}$ and $YbCo_6Sn_6$ [53,55]. The Co(1) atom is in a distorted $[Sn_5]$ square pyramidal geometry as in $DyCoSn_2$ and $Ce_4Co_2Sn_5$ [39,50].

$Yb_4Mn_2Sn_5$ crystallizes in the monoclinic space group *C*2/*m* with the Mg_5Si_6 structure type [60]. Its anionic substructure can be described as a 3D open framework built by parallel $[Mn_2Sn_2]$ ladders interconnected by novel zigzag $[Sn_3]$ chains, forming large tunnels along the *c*-axis (Fig. 4a). To the best of our knowledge, $Yb_4Mn_2Sn_5$ represents the first ordered ternary variant of Mg_5Si_6 with one Si site (4*i*) replaced by Mn, one Mg site (2*a*) substituted by Sn and the remaining Mg sites replaced by Yb atoms (Fig. 4c). Their structural formula can be written as $Yb_4[MnSn]_2[Sn_3]$ and $Mg_4Si_4[MgSi_2]$, respectively. $RE_4Ni_2InGe_4$ (RE = Dy, Ho, Er, Tm) can be considered the first quaternary ordered variant of Mg_5Si_6 where *RE* and In atoms occupy the Mg sites, and Ni and Ge atoms fill the Si sites [61].

The $[Mn_2Sn_2]$ ladder is formed by Mn(1) and Sn(3) atoms (Fig. 5a). The Mn–Sn distances of 2.790(2) and 2.791(3) Å are very close to those reported in $YbMn_6Sn_6$ [16]. The shortest Mn–Mn bond distances within the $[Mn_2Sn_2]$ ladders are 3.142(4) Å, which is significantly longer than the sum of Pauling's single bond radii of 2.50 Å [62].

The unique $[Sn_3]$ chain can be viewed as the linear $[Sn_3]$ trimers being interconnected in the head to tail fashion (Fig. 5b). The linear $[Sn_3]$ trimer is formed by one Sn(2) atom as the center and two Sn(1) atoms with Sn(1)–Sn(2) distance of 3.117(1) Å, which is slightly longer than those of the Sn–Sn bonds in the zigzag Sn chains in Yb_3CoSn_6 (2.945(2) Å and 3.071(3) Å). The Sn(1)–Sn(1) bond (2.819(2) Å) is significantly shorter than Sn(1)–Sn(2) bond. So the zigzag $[Sn_3]$ chain can also be considered as the Sn(2) atoms serving as bridges for the $[Sn(1)_2]$ dimeric units with Sn(1)–Sn(1)–Sn(2) angle of 109.46(6)°. Such $[Sn_3]$ chain is

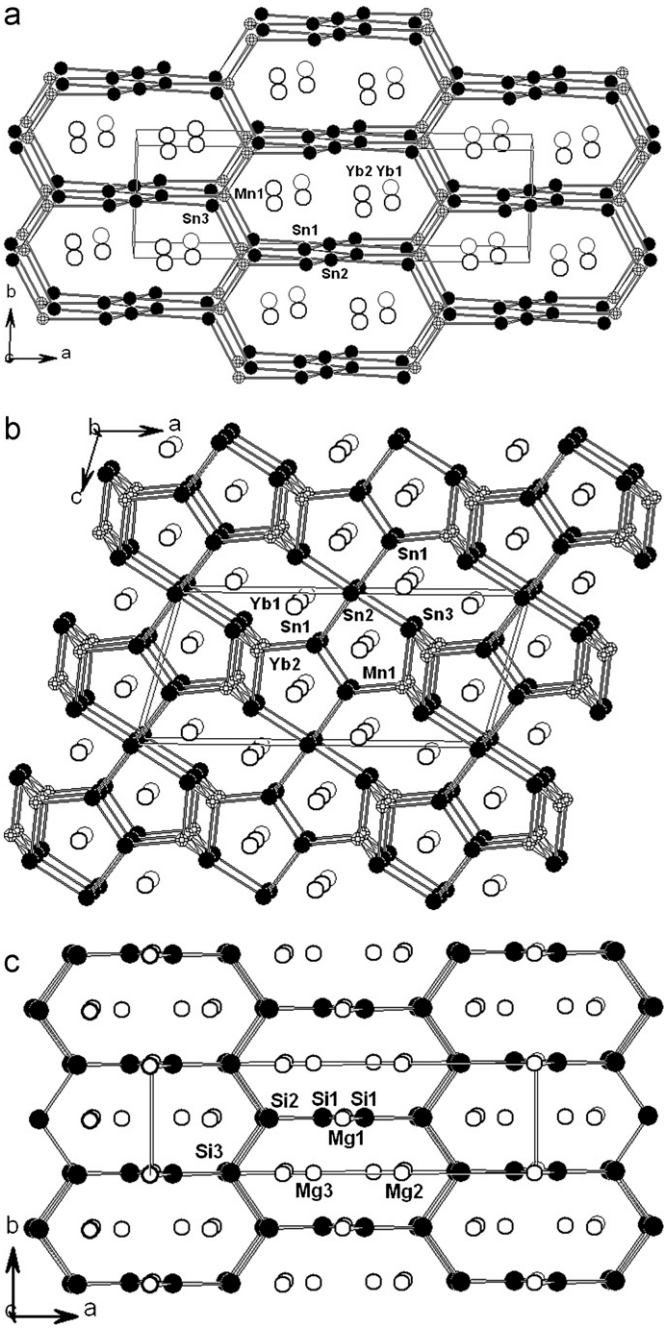

Fig. 4. View of the structure of $Yb_4Mn_2Sn_5$ along the *c*-axis (a) and the *b*-axis (b) and its comparison with that of Mg_5Si_6 (c).

different from the zigzag tin chains in Yb_3CoSn_6 and Lu_2NiSn_6, but is similar to the $[MgSi_2]$ chain in Mg_5Si_6 and the $[InGe_2]$ chain in $Ho_4Ni_2InGe_4$ [60,61].

The parallel $[Mn_2Sn_2]$ ladders and zigzag $[Sn_3]$ chains are further interconnected via Mn(1)–Sn(1) and Sn(2)–Sn(3) bonds into a novel 3D $[Mn_2Sn_5]$ open framework, forming long-narrow-shaped tunnels along the *c*-axis which are occupied by the Yb cations (Fig. 4a). Viewing down the *b*-axis, two types of tunnels are observed, the smaller one is formed by $[MnSn_4]$ 5-membered rings and the larger one is formed by $[Mn_2Sn_6]$ 8-membered rings. Yb(1) atoms are located at larger tunnels whereas Yb(2) atoms occupy the smaller ones (Fig. 4b). Yb(1) is 10-coordinated by two Sn(1), two Sn(2), three Sn(3) atoms and three Mn(1) atoms, whereas Yb(2) is 11-coordinated by four Sn(1), two Sn(2), two

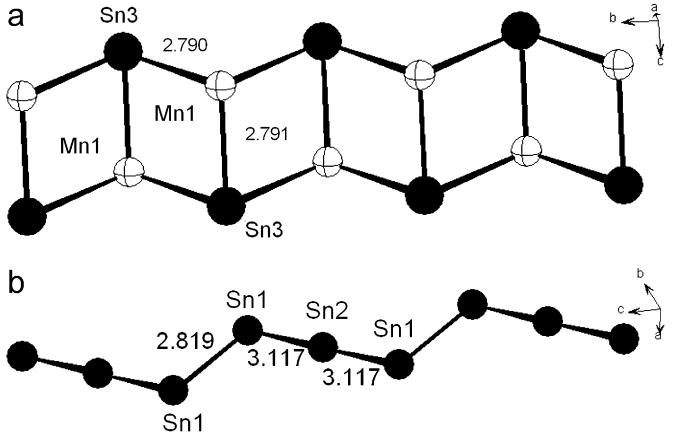

Fig. 5. The $[Mn_2Sn_2]$ ladder along the *b*-axis (a) and unusual $[Sn_3]$ chain along the *c*-axis (b) in $Yb_4Mn_2Sn_5$.

Sn(3) atoms and three Mn(1) atoms. The Yb–Sn bond lengths are in the range of 3.158(1)–3.5724(7) Å, which are comparable with those in Yb_3CoSn_6. The Yb–Mn distances fall in the range of 3.322(3)–3.806(2) Å. The Mn atom in $Yb_4Mn_2Sn_5$ has a slightly distorted tetrahedral coordination environment, such type of coordination geometry can also be found in $PrMn_{0.5}Sn_{1.83}$ [63].

3.2. Structural relationships

It is interesting to compare the structure of Yb_3CoSn_6 with that of $DyCoSn_2$ [39]. Both compounds crystallize in the orthorhombic space group *Cmcm* (no. 63). Comparing their cell parameters, it is noticed that $aD_yCoSn_2 \approx aYb_3CoSn_6$ and $bD_yCoSn_2 \approx bYb_3CoSn_6$, but $3cD_yCoSn_2 \approx cYb_3CoSn_6$. The differences between their cell parameters are comparable with their structural characters. All Sn_4 square sheets in $DyCoSn_2$ are capped by Co atoms to form a [CoSn] layer, and such layers are interconnected by the zigzag Sn chains into a 3D open framework. Furthermore, a series of $RETM_{0.33}Sn_2$ (or RE_3CoSn_6) phases (TM = Mn, Fe, Co) of $CeNiSi_2$ structure type have been previously determined by photographic powder method, in which transition metal site is disordered and displays defects [64,65]. Yb_3CoSn_6 can be viewed as the three-fold superstructure of $CeNiSi_2$ type, in which two thirds of Co atoms capping the Sn square-nets are vacant.

It is also interesting to compare the structure of $Yb_4Mn_2Sn_5$ with $Ce_4Co_2Sn_5$ [50]. These compounds crystallize in the same monoclinic space group and have a similar chemical composition, however, their unit cell dimension and structural characters are completely different. $Ce_4Co_2Sn_5$ and $Yb_4Mn_2Sn_5$ all contain $[TM_2Sn_2]$ ladder and $[Sn_2]$ dimeric units. For $Ce_4Co_2Sn_5$, the $[Co_2Sn_2]$ ladders are connected by other Sn atoms form 2D $[Co_2Sn_3]$ layers, which are further linked by $[Sn_2]$ dimer to form a 3D $[Co_2Sn_5]$ framework. Whereas for $Yb_4Mn_2Sn_5$, the $[Mn_2Sn_2]$ ladders are parallel to each other and are interconnected by unusual $[Sn_3]$ chains made of $[Sn_3]$ trimers.

3.3. Band structure calculations

The electronic band structures of Yb_3CoSn_6 and $Yb_4Mn_2Sn_5$ are also investigated by using the FP-LAPW+lo method with the PBE-GGA approximation. The calculated total and partial density of states (DOS) as well as the band structures along high symmetry directions in the first Brillouin zone are given in Figs. 6 and 7, respectively.

It is seen that the valence band crosses the Fermi level with no visible band gap from the band structure, which means that Yb_3CoSn_6 exhibits the metallic character (Fig. 6a). The spin splitting has not occurred in Yb_3CoSn_6. From the calculated total and partial DOS with no spin-polarization (Fig. 7a), the states in the energy range of −10 to −6 eV are essentially dominated by Sn 5*s* electrons, the states just below the Fermi level are mainly contributed by the Yb 4*f*, Co 3*d* and Sn 5*p* electrons as well as a small amount of *s* electrons of Sn and Yb, and the states above the Fermi level mainly result from 5*d* of Yb. The acute peak of DOS just below the Fermi level is induced by the very local Yb 4*f* electrons. A strong hybridization between Co 3*d* and Sn 5*p* states is formed in the range of −4.5∼1.0 eV, and the DOS of three crystallographically different Sn atoms completely overlap between each other in the range of −10 to 0 eV, suggesting these two sorts of orbitals mixing should have a strong effect on the electronic properties of the compound. These specifics have been analyzed in detail and shown to play an important role and account for the metallicity of some intermetallics [66,67].

The electronic band structure of $Yb_4Mn_2Sn_5$ is different from that of Yb_3CoSn_6. From the band structure (Fig. 6b and c) and DOS (Fig. 7b), the electronic states of Yb 4*f* shift towards high energy level in $Yb_4Mn_2Sn_5$. There is a higher and more local peak of DOS (mainly resulted from Yb 4*f* states) at the Fermi level, appears more evident metallic characteristic than Yb_3CoSn_6. The contributions of Yb and Sn atoms for the total DOS are similar to those of Yb_3CoSn_6, whereas the Mn 3*d* orbitals show the large spin splitting, which is induced by the different symmetry and occupancy of electrons. The states with spin up are completely occupied while the states with spin down are almost emptied, which indicates a big spin magnetic moment in $Yb_4Mn_2Sn_5$. Similar to Yb_3CoSn_6, the Mn 3*d* states are also hybridized with Sn 5*p* states in the energy range of −4.5 to 1.5 eV. This characteristic, as well as the mixing between Yb 4*f* and Sn 5*p* orbitals near the Fermi level imply the itinerant behavior on the part of the electrons, which results in the metallic character of $Yb_4Mn_2Sn_5$. In addition, the covalent bonding interaction exists between the Sn atoms.

To visualize the nature of the bond character and to explain the charge transfer of Yb_3CoSn_6 and $Yb_4Mn_2Sn_5$, we have investigated the effect of the Co (Mn) and Sn states on the difference electron density $\Delta\rho$ maps. $\Delta\rho$ represents the difference between the crystalline electron density and the superposition of electron densities form the neutral atoms. In these figures, the curve lines around the atoms indicate those regions where the electron density is higher in the crystal than the superposition of neutral atoms [68]. The difference electron densities distribution for the *bc* plane ($x = 0$) in Yb_3CoSn_6 shows strong covalent contributions for all the Co–Sn interactions and nearest Sn–Sn contacts, which is greatly consistent with the calculated results of the DOS (Fig. 8a). It should be noted that three Co–Sn bonds are on the same charge density consistent with their similar bond lengths, and delocalized molecular orbitals exist among Sn atoms along the zigzag Sn chains. We also find that there are no evident bonds existing between Sn(3) atoms and Sn(1), Sn(2) atoms, which are in accord with their bond distances (Sn(3)–Sn(1): 3.492(1) Å and Sn(3)–Sn(2): 3.406(1) Å).

The Mn–Sn and Sn–Sn bonds also show the strong interactions in $Yb_4Mn_2Sn_5$ according to the calculated difference electron densities distribution along the *ac* plane ($y = 0$), which is similar to those in Yb_3CoSn_6 (Fig. 8b). It should be noted that the difference electron density distribution also shows the presence of lone pairs for the Sn(1) atoms, which is consistent with their coordination environments. These characters have been analyzed in detail and shown to play an important role and account for the electrical conductivities of some intermetallics, such as $SrSn_3$, $SrSn_4$, $BaSn_5$ and so on [11–14]. Comparing with the Sn–Sn bonds and Co (Mn)–Sn bonds, there is a little difference electron density around Yb atom in the directions toward Co (Mn) and Sn atoms.

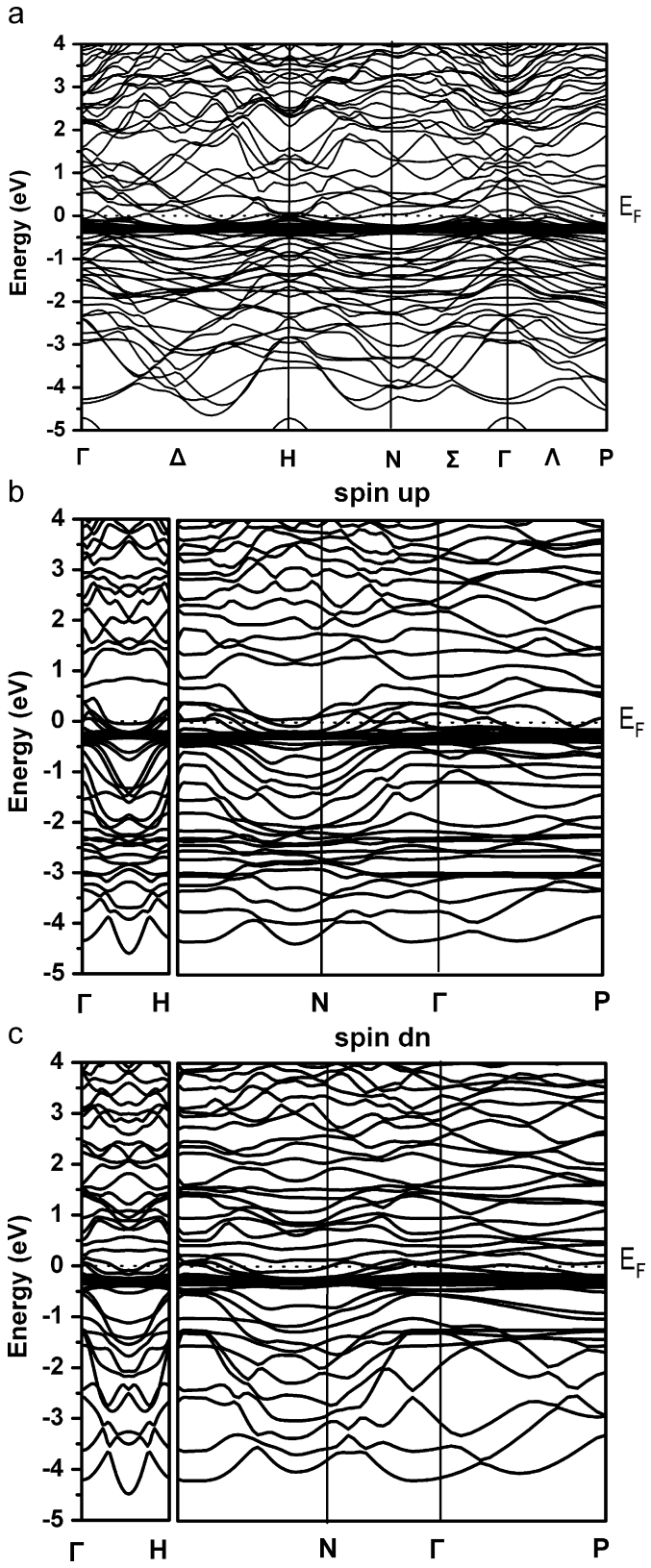

Fig. 6. Calculated band structures for Yb_3CoSn_6 (a), and the spin up (b) and spin down (c) of the band structures of $Yb_4Mn_2Sn_5$. Γ (0, 0, 0); H (1, 0, 0); N (0.5, 0.5, 0); P (0.5, 0.5, 0.5). The Fermi level is set at 0 eV.

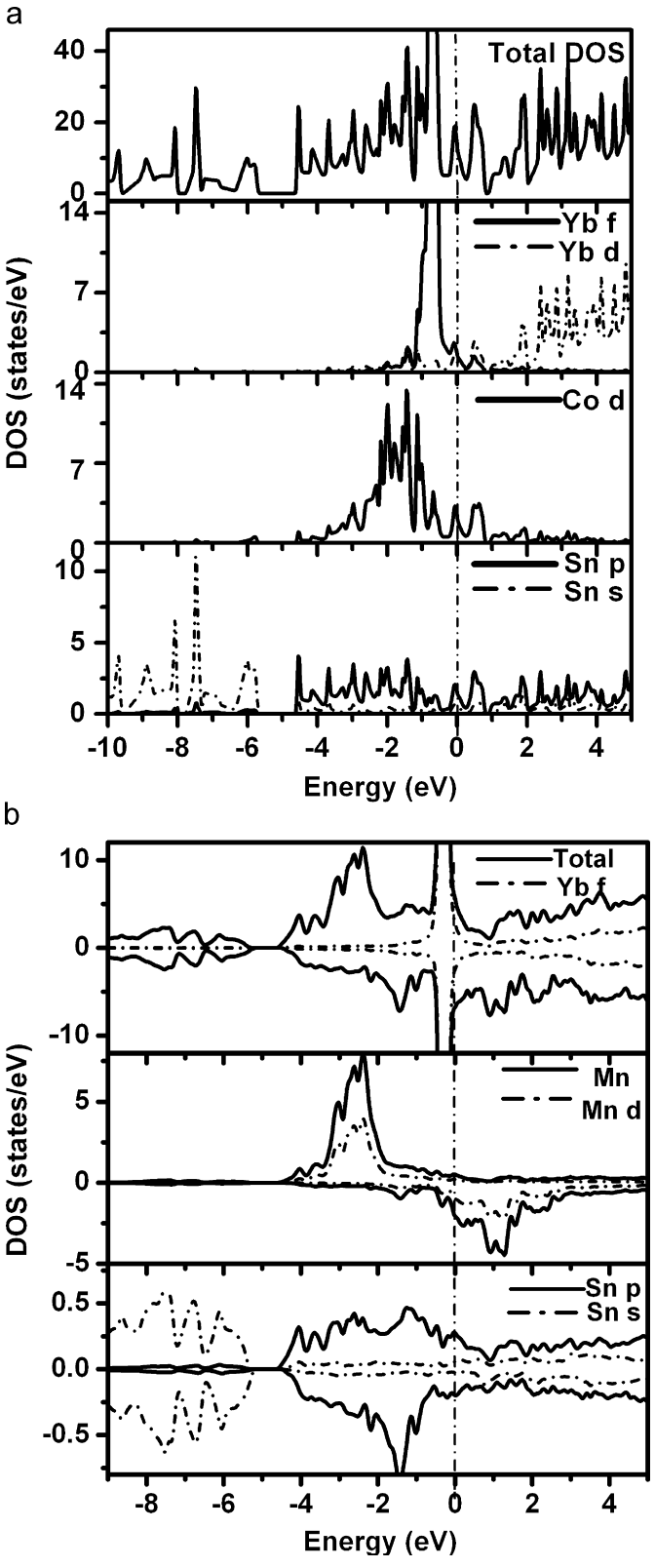

Fig. 7. Calculated total and partial density of states (DOS) of Yb_3CoSn_6 (a) and $Yb_4Mn_2Sn_5$ (b). The Fermi level is represented by the dotted line and is set at 0 eV.

This confirms the less covalent character between Yb and Sn, Co (Mn) atoms for Yb_3CoSn_6 and $Yb_4Mn_2Sn_5$, respectively. Such bond character is consistent with the results of the calculated DOS.

Furthermore, considering the local 3*d* and 4*f* electrons in these two compounds, we further perform the GGA+*U* (on-site coulombic energy correction)-type calculations to examine the

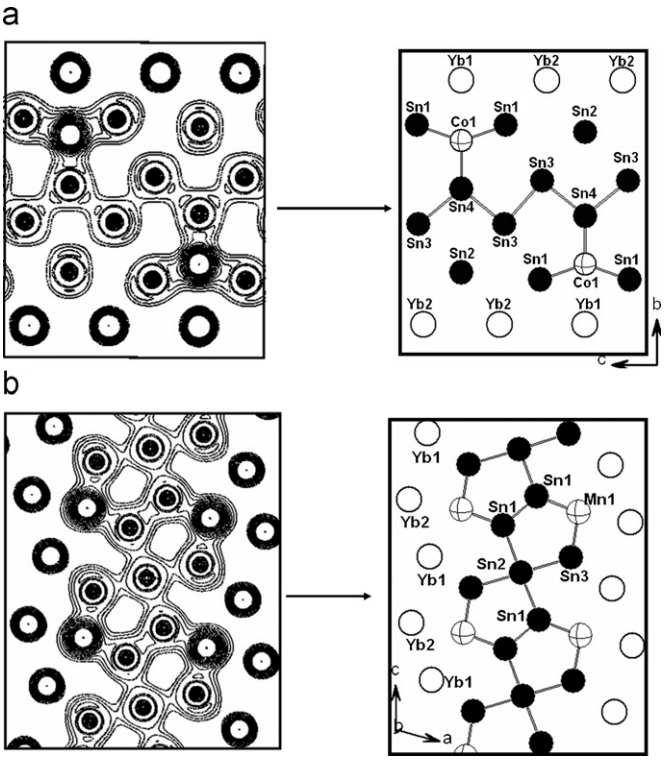

Fig. 8. Representation of the difference electron density ($\Delta\rho$) for *bc* plane with $x = 0$ cuts through the zigzag Sn chains in Yb_3CoSn_6 (a) and for *ac* plane with $y = 0$ cuts through the zigzag $[Sn_3]$ chains in $Yb_4Mn_2Sn_5$ (b). The contour intervals are in the units of 0.025 e Å^{-3}.

correlation of *d* or *f* electrons. As a result, we find that besides small quantitative changes, the qualitative picture described in this paper is unchanged. Namely, the *U* parameter does not influence the energy and DOS of both 3*d* and 4*f* electrons. It is shown that the correlation effect of 3*d* and 4*f* electrons is not strong in these two systems. Thus, the GGA exchange correlation formation can give sufficient and reliable results.

4. Concluding remarks

In summary, we have successfully obtained two new tin-rich ternary phases, Yb_3CoSn_6 and $Yb_4Mn_2Sn_5$. Their structures feature two types of 3D open frameworks: one is built from $[CoSn_3]$ layers interconnected by zigzag Sn chains whereas the other one is formed by the $[Mn_2Sn_2]$ interconnected by the unusual Sn chains made of linear Sn_3 trimers. The Co atom in Yb_3CoSn_6 adopts the distorted square pyramid coordination geometry whereas the Mn atom in $Yb_4Mn_2Sn_5$ is tetrahedrally coordinated. Both compounds are metallic based on electronic band structure calculations. Spin polarized DFT calculations also indicate that Yb_3CoSn_6 exhibits no spin splitting whereas $Yb_4Mn_2Sn_5$ is expected to be ferromagnetic. Future research efforts will be devoted to the syntheses, crystal and electronic structures as well as physical properties of the related phases of other lanthanide metals.

Acknowledgments

We thank the financial supports from the National Nature Science Foundation of China (nos. 20573113, 20731006, and 20521101).

Appendix A. Supplementary materials

The online version of this article contains additional supplementary data. Please visit doi:10.1016/j.jssc.2008.05.036.

References

[1] B. Eisenmann, G. Cordier, Chemistry, Structure and Bonding of Zintl Phases and Ions, VCH Publishers, New York, 1996, p. 61.
[2] J.D. Corbett, Chemistry, Structure and Bonding of Zintl Phases and Ions, VCH Publishers, New York, 1996, p. 139.
[3] J.D. Corbett, Angew. Chem. Int. Ed. 39 (2000) 670.
[4] T.F. Fässler, S. Hoffmann, Z. Kristallogr. 214 (1999) 722.
[5] M.G. Kanatzidis, K.R. Poeppelmeier, Prog. Solid State Chem. 36 (2007) 1–133.
[6] C. Lupu, J.-G. Mao, J.W. Rabalais, A.M. Guloy, Inorg. Chem. 42 (2003) 3765.
[7] F. Dubois, T.F. Fässler, J. Am. Chem. Soc. 127 (2005) 3264.
[8] J.T. Vaughey, J.D. Corbett, Inorg. Chem. 36 (1997) 4316.
[9] T.F. Fässler, C. Kronseder, Angew. Chem. Int. Ed. 37 (1998) 1571.
[10] E.A. Leon-Escamilla, J.D. Corbett, Inorg. Chem. 38 (1999) 738.
[11] T.F. Fässler, S. Hoffmann, Z. Anorg. Allg. Chem. 626 (2000) 106.
[12] T.F. Fässler, C. Kronseder, Angew. Chem. Int. Ed. 36 (1997) 2683.
[13] S. Hoffmann, T.F. Fässler, Inorg. Chem. 42 (2003) 8748.
[14] T.F. Fässler, S. Hoffmann, C. Kronseder, Z. Anorg. Allg. Chem. 627 (2001) 2486.
[15] S. Bobev, S.C. Sevov, J. Solid State Chem. 153 (2000) 92.
[16] S.S. Bobev, S.C. Sevov, Angew. Chem. Int. Ed. 39 (2000) 4108.
[17] A.K. Ganguli, J.D. Corbett, M. Köckerling, J. Am. Chem. Soc. 120 (1998) 1223.
[18] S. Bobev, S.C. Sevov, J. Am. Chem. Soc. 124 (2002) 3359.
[19] G.S. Nolas, B.C. Chakoumakos, B. Mahieu, G.J. Long, T.J.R. Weakly, Chem. Mater. 12 (2000) 1947.
[20] M. Beekman, G.S. Nolas, J. Mater. Chem. 18 (2008) 842.
[21] A.P. Wilkinson, C. Lind, R.A. Young, S.D. Shastri, P.L. Lee, G.S. Nolas, Chem. Mater. 14 (2002) 1300.
[22] G.S. Nolas, T.J.R. Weakley, J.L. Cohn, Chem. Mater. 11 (1999) 2470.
[23] R. Pöttgen, Z. Naturforsch. 61b (2006) 677.
[24] Z.-M. Sun, S.-Q. Xia, Y.-Z. Huang, L.-M. Wu, J.-G. Mao, Inorg. Chem. 44 (2005) 9242.
[25] M.L. Fornasini, P. Manfrinetti, D. Mazzone, P. Riani, G. Zanicchi, J. Solid State Chem. 177 (2004) 1919.
[26] M.L. Fornasini, G. Zanicchi, D. Mazzone, P. Riani, Z. Kristallogr. NCS 216 (2001) 21.
[27] S. Singh, S.K. Dhar, P. Manfrinetti, A. Palenzona, J. Alloys Compds. 298 (2000) 68.
[28] W. Dörrscheidt, H. Schäfer, J. Less-Common Met. 58 (1978) 209.
[29] M. Boudard, B. Doisneau, F. Audebert, J. Alloys Compds. 370 (2004) 169.
[30] D.A. Vennos, M.E. Badding, F.J.J. Disalvo, J. Less-Common Met. 175 (1991) 339.
[31] B. Chevalier, J.J. Etourneau, Mater. Chem. 9 (1999) 1789.
[32] M.A. Zhuravleva, D. Bilc, S.D. Mahanti, M.G. Kanatzidis, Z. Anorg. Allg. Chem. 629 (2003) 327.
[33] Z.-M. Sun, D.-C. Pan, X.-W. Lei, J.-G. Mao, J. Solid State Chem. 179 (2006) 3378.
[34] S. Cirafici, F. Canepa, P. Manfrinetti, M. Napoletano, J. Alloys Compds. 317–318 (2001) 550.
[35] F. Canepa, M. Napoletano, P. Manfrinetti, S. Cirafici, J. Alloys Compds. 314 (2001) 29.
[36] F. Canepa, S. Cirafici, M.L. Fornasini, P. Manfrinetti, F. Merlo, A. Palenzona, M. Pani, J. Alloys Compds. 297 (2000) 109.
[37] R. Pöttgen, J. Alloys Compds. 224 (1995) 14.
[38] S.-Q. Xia, S. Bobev, Acta Crystallogr. E 62 (2006) 17.
[39] A. Gil, B. Penc, E. Wawrzyńska, J. Hernandez-Velasco, A. Szytuła, A. Zygmunt, J. Alloys Compds. 365 (2004) 31.
[40] A. Gil, B. Penc, S. Baran, J. Hernandez-Velasco, A. Szytula, A. Zygmunt, J. Alloys Compds. 361 (2003) 32.
[41] P. Schobinger-Papamantellos, J. Rodríguez-Carvajal, G.H. Nieuwenhuys, L.W.F. Lemmens, K.H.J. Buschow, J. Alloys Compds. 262 (1997) 335.
[42] CrystalClear version. 1. 3. 5; Rigaku Corp., Woodlands, TX, 1999.
[43] G.M. Sheldrick, SHELXTL, Crystallographic Software Package, Version 5.1, Bruker-Axs, Madison, WI, 1998.
[44] G.K.H. Madsen, P. Blaha, K. Schwarz, E. Sjöstedt, L. Nordström, Phys. Rev. B 64 (2001) 195134.
[45] K. Schwarz, P. Blaha, G.K.H. Madsen, Comput. Phys. Commun. 147 (2002) 71.
[46] J.P. Perdew, K. Burke, M. Ernzerhof, Phys. Rev. Lett. 77 (1996) 3865.
[47] P. Blaha, K. Schwarz, G.K.H. Madsen, D. Kvasnicka, J. Luitz, WIEN2k, An Augmented Plane Wave + Local Orbitals Program for Calculating Crystal Properties (Karlheinz Schwarz, Techn. Universität Wien, Austria), 2001, ISBN:3-9501031-1-2.
[48] J. Donohue, The Structures of the Elements, Wiley, New York, 1974.
[49] B. Eisenmann, H. Schäfer, Z. Anorg, Allg. Chem. 403 (1974) 163.
[50] M. Pani, P. Manfrinetti, A. Palenzona, S.K. Dhar, S. Singh, J. Alloys Compds. 299 (2000) 39.
[51] M. Schreyer, T.F. Fässler, Solid State Sci. 8 (2006) 793.
[52] E.L. Thomas, H.-O. Lee, A.N. Bankston, S. MaQuilon, P. Klavins, J.Y. Chan, J. Solid State Chem. 179 (2006) 1641.
[53] Y. Mudryk, A. Grytsiv, P. Rogl, C. Dusek, A. Galatanu, E. Idl, H. Michor, E. Bauer, C. Godart, D. Kaczorowski, L. Romaka, O. Bodak, J. Phys.: Condens. Matter. 13 (2001) 7391.
[54] M. Schreyer, G. Kraus, T.F. Fässler, Z. Anorg. Allg. Chem. 630 (2004) 2520.

[55] L. Romaka, Y. Mudryk, Y. Stadnyk, P. Rogl, L. Akselrud, in: Fifteenth International Conference on Solid Compounds of Transition Elements, Krakow, Poland, 2006, p. 12.
[56] O. Nial, Z. Anorg. Allg. Chem. 238 (1938) 287.
[57] E.E. Havinga, P. Hokkelin, H. Damsma, J. Less-Common Met. 27 (1972) 169.
[58] H. Rajeswar, H. Manohar, Indian J. Pure Appl. Phys. 8 (1970) 363.
[59] A. Palenzona, P. Manfrinetti, M.L. Fornasini, J. Alloys Compds. 280 (1998) 211.
[60] S.J. Andersen, H.W. Zandergen, J. Jansen, C. Traeholt, U. Tundal, O. Reiso, Acta Mater. 46 (1998) 3283.
[61] J.R. Salvador, M.G. Kanatzidis, Inorg. Chem. 45 (2006) 7091.
[62] L. Pauling, B. Kamb, Proc. Natl. Acad. Sci. USA 83 (1986) 3569.
[63] A. Gil, A. Oleś, W. Sikora, A. Szytuła, J. Alloys Compds. 360 (2003) 21.
[64] R.V. Skolozdra, Yu.K. Gorelenko, E.E. Terletskaya, V.D. Tkachuk, Fizika Metallov i Metallovedenie 66 (5) (1988) 864.
[65] R.V. Skolozdra, in: K.A. Gschneidner, L. Eyring (Eds.), The Handbook of the Physics and Chemistry of Rare Earths, Elesvier, Amsterdam, 1997 Chapter 164.
[66] S.H. Devon Moore, L. Deakin, M.J. Ferguson, A. Mar, Chem. Mater. 14 (2002) 4867.
[67] A.M. Mills, A. Mar, J. Am. Chem. Soc. 123 (2001) 1151.
[68] M. Iglesias, K. Schwarz, P. Blaha, D. Baldomir, Phys. Chem. Miner. 28 (2001) 67.